Average Structure vs. Real Structure: Molecular Dynamics Studies of Silica

M. H. Müser

Institut für Physik, Johannes Gutenberg-Universität, Mainz, Germany

Abstract. The microscopic structure of a crystal and thermal fluctuations of the atoms constituting the crystal are intimately connected with the macroscopic elastic properties including mechanical stability. In some cases, however, the picture is more complex than that which is drawn in text books on solid state physics. (i) The instantaneous microscopic structure can deviate in a non-Gaussian way from the average structure even when domain disorder and/or crystal defects are absent. Quasi harmonic approximations may then turn out to be meaningless. (ii) The crystal is subject to external pressures that are sufficiently large in order to render the definition of elastic constants non unique. These two points are discussed exemplarily in the context of the high-temperature and the high-pressure phases of quartz. In particular, it is discussed how to observe and how to classify non-Gaussian disorder in molecular dynamics (MD) simulations and how to evaluate mechanical stability of solids under pressure. Some details are given on the calculation of thermal, mechanical, and structural properties of solids, also for temperatures far below their Debye temperature.

1 Introduction

Pure silica (SiO_2) has a rich phase diagram with interesting temperature and pressure induced phase transitions between the various stable or metastable polymorphs[Dolino 1990], [Heaney, Prewitt, and Gibbs 1994]. The large variety of crystalline phases is due to the tetrahedral structure of relatively rigid SiO_4 units and the large geometric flexibility with which they can be connected. The material properties in general and the mechanisms driving the phase transition in particular are often explained in terms of their average structure and (Gaussian) fluctuations around this average structure. Detailed molecular dynamics simulations reveal that the picture needs to be refined [Müser and Binder 2001]: In the high-temperature phases, e.g., in β-quartz, the fast oscillations of oxygen atoms are around (time-dependent) positions that do not correspond to the ideal oxygen positions in β quartz. The averaged configurations only resemble the ideal structure if averaged over time scales that are distinctly larger than typical inverse phonon frequencies. This effect has serious implications on the calculation of material properties: The calculation of elastic constants as evaluated in terms of a quasi-harmonic approximation turns out to be meaningless.

Another controversially discussed phase transition of quartz is the pressure-induced transformation of α-quartz into quartz-II [Kingma et al. 1993]. Based on a mechanical stability analysis by means of molecular dynamics (MD) simulations, Binggeli and Chelikowsky (1992) suggested that the transformation is induced by an elastic instability. The MD predictions were in contradiction with an experimental mechanical stability analysis by Gregoryanz et al. (2000). The discrepancy between simulation and experiment may not be due to poor MD modeling but it may rather be due to the ambiguity in defining elastic constants for solids under large pressure [Müser and Schöffel 2001]. Of course, the correct stability criterion must require that the long-range structural fluctuations are finite.

In these lecture notes, a selective review on MD simulations of various quartz modifications and the phase transformations between them is given. In particular, it is emphasized what a computer simulation should provide in order to be compared to experiments and in order to make predictions that complement reliably experimental observations. The potential energy surfaces suggested by van Beest, Kramer, and van Santen (1990) is used as their two-body potential turned out to describe rather accurately various aspects of silica in different crystalline phases [Tse and Klug 1991].

2 Molecular Dynamics Simulations of Crystals

The code for a molecular dynamics (MD) simulation [Allen and Tildesley 1987], [Frenkel and Smit 1996] or a Monte Carlo (MC) [Landau and Binder 2000] simulation of a crystal is of course similar to that of any system which is described in terms of effective or *ab initio*-based interatomic potentials. In principle, the starting point is a Lagrangian L

$$L = \sum_{n=1}^{N} \frac{1}{2} m_n \dot{\mathbf{R}}_n^2 - V(\{R\}), \tag{1}$$

where m_n denotes the mass of particle n and $V(\{R\})$ is the net potential energy as a function of the coordinates of all N particles. The well-known Newton equation's of motion for the particles are derived from L. These equations are integrated numerically, stepping forward in time by discrete steps of size Δt. To thermostat the system, the equations of motion are modified so that the average kinetic energy stays at its equilibrium value. There are various approaches to achieve this. An efficient way that also works without modifications for strongly harmonic systems (note that the famous Nosè-Hoover thermostat suffers from serious difficulties for such systems!) is to couple each atom to its own local thermostat [Schneider and Stoll 1978]. The exchange of energy with the outside world is modeled by a Langevin equation that includes a damping coefficient γ and a random force $\mathbf{\Gamma}_n(t)$ on each atom. The equations of motion for the α

component of the position $R_{n\alpha}$ become:

$$m_n \frac{d^2 R_{n\alpha}}{dt^2} = -\frac{\partial}{\partial R_{n\alpha}} V(\{R\}) - m_n \gamma \frac{dR_{n\alpha}}{dt} + \Gamma_{n\alpha}(t). \tag{2}$$

In order to satisfy the fluctuation-dissipation theorem, the $\Gamma_{n\alpha}(t)$ must be completely random, have zero mean, and have a second moment given by

$$\langle \Gamma_{n\alpha}(t) \Gamma_{n'\beta}(t') \rangle = 2 k_{\mathrm{B}} T \gamma m_n \delta_{nn'} \delta_{\alpha\beta} \frac{\delta_{tt'}}{\Delta t}. \tag{3}$$

Note that Eq. (3) is written down for a discretized time.

While the remarks above are generally valid, there are two important points that are usually more relevant for crystals than for fluids or other disordered systems. (i) The crystal structure may not be conform with a periodically repeated simulation box of orthorhombic symmetry. This makes it necessary to employ arbitrary parallelepiped shaped simulation boxes. Such geometries also enable us to calculate all elastic constants from thermal strain fluctuations. (ii) Quantum effects typically play a more significant roles in crystals than in fluids, although fluid helium is a prominent exception of this rule. Ways to incorporate these two points into MD simulations will now be discussed in further detail.

2.1 MD for arbitrary parallelepiped simulation cells

The simulation of crystals in an arbitrarily parallelepiped shaped simulation cell goes back to an idea invoked by a series of papers by Parrinello and Rahman (1980, 1981, and 1982): The atomic positions are represented as a scalar product of a dimensionless vector $\mathbf{r}$ (with components between zero and unity) with a (symmetric!) matrix h whose rows are parallel to the three edges spanning the simulation cell:

$$R_{n,\alpha} = \sum_{\beta=1}^{3} h_{\alpha\beta}\, r_{n,\beta}. \tag{4}$$

The Lagrangian described in Eq. (1) is then generalized by also attributing inertia to the simulation cell's geometry and by coupling the simulation cell's volume $\det(\mathsf{h})$ to an isotropic pressure p:

$$L\left(\mathsf{h}, \dot{\mathsf{h}}, \{\mathsf{r}\}, \{\dot{\mathsf{r}}\}\right) = \sum_{\alpha\beta} \frac{1}{2} W \dot{h}_{\alpha\beta}^2 + \sum_{n=1}^{N} \frac{1}{2} m_n (\mathsf{h}\dot{\mathbf{r}}_n)^2 \; - V(\{\mathsf{h}r\}) - p \det(\mathsf{h}). \tag{5}$$

Note that the original Lagrangian is recuperated by setting $\dot{\mathsf{h}}$ to zero and that the choice of the inertia term W is not unique, because this term can not be determined from first principles. While the choice of W affects the dynamics of the system, it does not affect the distribution functions of h and $\{\mathbf{r}\}$.

Using the Lagrangian formalism, the equations of motion for h and $\{\mathbf{r}\}$ can be derived in a straightforward way. It is convenient to thermostate all variables in order to have quickly converging ensemble averages. The choice of a Langevin type thermostat for h is particularly helpful as these modes are usually strongly harmonic and hence couple only weakly to the inner degrees of freedom $\{\mathbf{r}\}$.

In order to define the strain tensor ϵ, we need to know the thermal expectation value $\mathsf{h}_0 = \langle \mathsf{h} \rangle$. ϵ is given by

$$\epsilon = \frac{1}{2}\left({\mathsf{h}_0'}^{-1} \mathsf{h}' \mathsf{h} {\mathsf{h}_0}^{-1} - 1 \right). \tag{6}$$

Thus by monitoring the various moments of h in the simulation, it is possible to calculate the first and the second moment of the thermal strain fluctuations $\delta\epsilon$ from which the (isothermal) elastic constants $C^T_{\alpha\beta\gamma\delta}$ follow via:

$$(C^T)^{-1}_{\alpha\beta\gamma\delta} = \frac{\det(\mathsf{h}_0)}{k_B T} \langle \delta\varepsilon_{\alpha\beta} \delta\varepsilon_{\gamma\delta} \rangle . \tag{7}$$

If this fluctuation relation is applied to non-zero pressures, then the $C_{\alpha\beta\gamma\delta}$ correspond to Birch coefficients rather than to elastic constants. This point will be further elucidated in Section 5. In any case, Eq. (7) is a manifestation of the connection between structure fluctuations and elastic properties.

2.2 MD below the Debye temperature

Path integral Monte Carlo (PIMC) [Barker 1979] and path integral molecular dynamics (PIMD) [Tuckerman et al. 1993] have proven useful in the atomistic simulation of quantum effects occurring in condensed matter at low temperatures (see also the article by Gernoth in these Lecture Notes). The application of path integral simulations is not restricted anymore to the calculation of thermal and structural properties of Lennard-Jones type systems but the treatment of more complex condensed matter systems becomes increasingly feasible.

In order to derive the path-integral scheme for a system with fluctuating simulation cell size, it is convenient to start from the Lagrangian given in Eq. (5). One should not quantize the tensor h, because in the long-wavelength limit this quantity becomes always classical and because the choice of the inertia W is arbitrary. Thus the quantization of the variables $\mathbf{r}_n$ can be achieved as usual. Path integral simulations exploit Feynman's idea to represent the partition function of a quantum mechanical point particle $Z(\beta)$ as a partition function of a classical ring polymer [Feynman and Hibbs 1965]. The position of a quantum mechanical point particle is represented by a chain with coordinates $\mathbf{r}_t$ with $t = 1, ..., P$ and cyclic boundary conditions $\mathbf{r}_t = \mathbf{r}_{t+P}$. In the present notation, the partition function reads:

$$Z(\beta) = \lim_{P\to\infty} \frac{[\det(\mathsf{h})]^{NP}}{\prod_{n=1}^{N} \lambda_n^{3P}(\beta/P)} \prod_{n=1}^{N} \prod_{t=1}^{P} \int_0^1 d^3 r_{n,t} e^{-\beta V_{\mathrm{rp}}/P} \tag{8}$$

with

$$V_{\mathrm{rp}}(\{R\}) = \sum_{t=1}^{P} \left[V(\mathbf{R}_{1,t}, ..., \mathbf{R}_{N,t}) + \frac{1}{2} \sum_{n=1}^{N} \frac{m_n P^2}{\beta^2 \hbar^2} \left(\mathbf{R}_{n,t} - \mathbf{R}_{n,t+1}\right)^2 \right], \qquad (9)$$

where the relation between $\mathbf{r}_n$ and large $\mathbf{R}_n$ is given as usual by Eq. (4). V represents the (real) potential energy of the system evaluated for particle coordinates at "imaginary time" t and the last summand of the right-hand side of Eq. (9) reflects the harmonic springs that keeps monomer of the ring polymer close together. It is instructive to visualize the interactions described in Eq. (9), which is done in Figure 1.

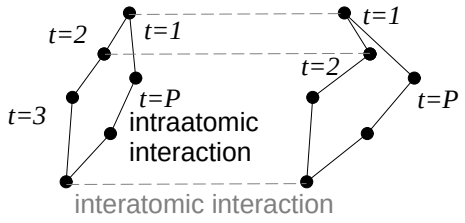

Figure 1: Illustration of the interaction between two quantum mechanical point particles that are represented as classical ring polymers.

The spring constants k_n connecting neighboring beads within a chain are given by $k_n = m_n P^2/\beta^2\hbar^2$. Hence large temperatures and/or large masses lead to a localization of the ring particle and thus to classical behaviour. The spatial extension of the chains at low temperatures reflects the thermal de Broglie wavelength.

In the quantum limit $P \to \infty$, the k_n become very stiff. This would lead to technical difficulties in a PIMD simulation if the "kinetic" masses of the beads were all chosen to be identical, because there would be a time scale separation between the center-of-mass mode and the internal modes. This effect would automatically result in an inefficient sampling, which is why one needs to come up with more efficient algorithm [Tuckerman et al. 1993]. One possibility is to attribute the inert masses (note that the real, physically meaningful masses are reflected in the harmonic springs) to the eigenmodes of the free chain and to chose them such that internal eigenfrequencies and typical frequencies associated with the center-of-mass motions are similar [Müser 2001]. For a proper choice of these masses including W and a proper choice for the Langevin damping coefficient γ, it is possible to obtain quickly converging estimates of many thermal and structural properties including the elastic constants.

3 Quantum effects in α-quartz

Many potential energy surfaces are adjusted such that they yield the proper lattice constants (parameters) and the correct elastic properties at low temperatures. This is also the case for the so-called BKS potential suggested for SiO_2 by van Beest, Kramer, and van Santen (1990). It is therefore an important test for a model potential surface to yield the correct thermal expansion at low temperature, because the anharmonic interactions are not explicitly incorporated into the potential parameters. Such a test requires a quantum mechanical treatment of the ionic motion, since classical expansion coefficients α remain finite as the temperature T tends to zero, while for a quantum mechanical treatment - like in experiment - α vanishes as T approaches zero. Despite the existence of sophisticated quasi-harmonic theories, it remains a challenge to predict reliably lattice parameters near absolute zero. Path integral simulations like PIMD, however, achieve very good resolution down to temperatures well below the Debye temperature T_D without any uncontrolled approximations other than the uncertainties due to the potential energy surface. Of course, these uncertainties would also be present in theoretical treatments.

Quartz has two independent lattice constants, a and c, with a and c representing the lattice parameters parallel to the x and z-direction respectively (in the standard representation). It turns out that thermal expansion is very well reproduced by the BKS potential at very low temperatures as can be seen in Figure 2, while classical simulations show the wrong trend at small T.

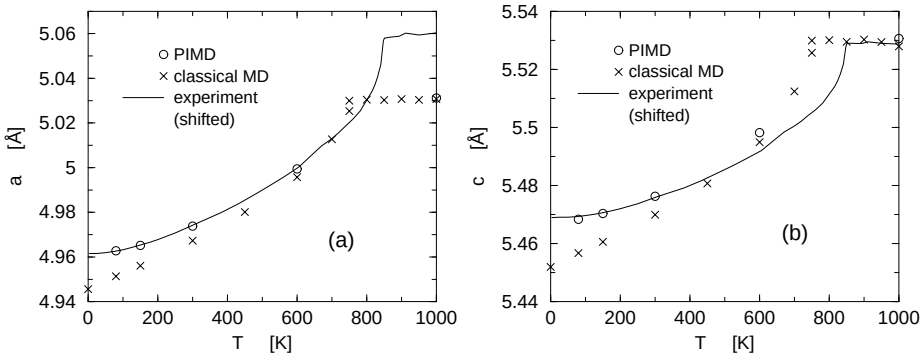

Figure 2: Lattice constants of α-quartz at ambient pressure as a function of temperature. a) Experimental values for the a-axis are shifted to larger values by 0.06 $\AA$. b) Experimental values for the c-axis are shifted to larger values by 0.07 $\AA$. Error bars of simulations in all cases smaller than 100 fm. Experiment taken from Carpenter et al. (1998). From Müser (2001).

Some numerical approaches (like density functional theory or other quantum chemistry approaches) reach a nearly perfect agreement with experiment,

especially for structural properties. In general, such calculations do not include quantum effects of the ionic motion. As we just saw, quantum effects lead to an equilibrium structure that slightly differs from the "classical" equilibrium structure. From Figure 2 we can learn that a highly accurate calculation should actually underestimate the experimentally measured lattice parameters for quartz near absolute zero by about 0.35 %. Of course, finite-temperature simulations also provide important tests, i.e., one observes a discrepancy in the α-β phase transition temperature of nearly 100 K and more importantly, the jump in the lattice parameter a is strongly suppressed in the simulation. These shortcomings are discussed elsewhere [Müser and Binder 2001].

A further phenomenon which needs quantum effects of the ionic motion to be considered are the well known isotope effects. E.g., for rare gas crystals such as ^{20}Ne and ^{22}Ne systematic differences between the lattice parameters were measured. The differences were rather nicely reproduced by path integral Monte Carlo simulations [Müser et al. 1995]. However, isotope effects will not be discussed here further.

The analysis of the influence of quantum mechanical effects is not limited to structural or thermal properties. With current computers and algorithms, it has also become possible to estimate elastic constants quite accurately, see i.e. the treatment of solid ^{3}He by Schöffel and Müser (2001). It seems a general trend that the *relative* corrections due to the quantum mechanical nature of ionic motion to cohesion energies (near $T = 0$ K) is larger than those to the lattice parameters and that the relative corrections to elastic constants is again larger than but in the same order as those to the cohesion energy. In α-quartz, the quantum induced reduction in the elastic constant C_{33} was estimated to be close to 5 GPa, which seems surprisingly large given the strong ionic-covalent bond in quartz and the relatively large masses of the constituting atoms. Figure 3 shows the elastic constants of α-quartz for a classical treatment, the quantum mechanical treatment along with some available experimental data.

Although this is hardly recognizable from the figure (because of the large scale needed for the ordinate), the temperature dependence of elastic constants calculated classically is qualitatively wrong: classical statistical mechanics always yields $\partial C_{ij}/\partial T \to$ const. as $T \to 0$ and this constant will in general be nonzero. Quantum mechanics requires $\partial C_{ij}/\partial T \to 0$ as $T \to 0$ due to the third law of thermodynamics.

From Figure 3 it is noticeable that the elastic constants measured experimentally at 300 K match the elastic constants from the classical simulations at zero temperature. This is due to the fact that the BKS potential was constructed such that ab-initio calculations were combined with bulk properties in order to fit the free model parameters. In the latter part, lattice constants and elastic constants were calculated for a classical system at $T = 0$ K from the (fit) parameters and adjusted such that agreement with experimental "quantum mechanical" (finite temperatures) data was optimum. While I consider the BKS potential to be the best two-body potential available for the simulation of bulk SiO_2, one can see

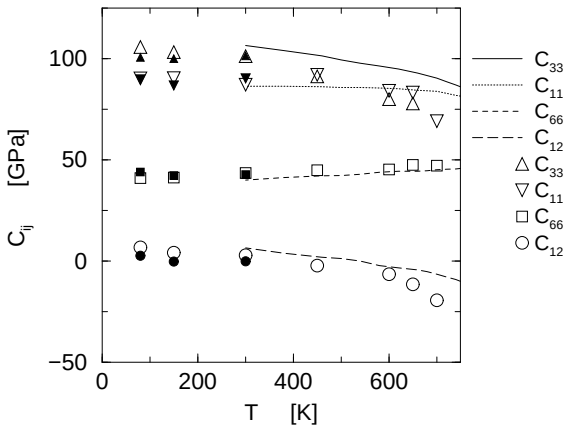

Figure 3: Various elastic constants. Experimental data shown as curves is taken from Carpenter et al. (1998). Open symbols refer to classical simulations, filled symbols to PIMD simulations. Statistical error bars are about 2 GPa. From Müser (2001).

that there is still some room left for improvement of the potential parameters.

It is interesting to note that T_{D} of α-quartz as determined by specific heat measurements [Striefler and Barsch 1975] is a strongly temperature-dependent function: At $T = 0, T_{\mathrm{D}} \approx 550$ K, while at room temperature $T_{\mathrm{D}} \approx 1,000$ K. This unusual behaviour can be understood if one keeps in mind the relevant degrees of freedom: There are low-lying excitations associated with so-called rigid unit modes (RUM) [Axe and Shirane 1970]. The RUM's are (collective) motions of stiff tetrahedral SiO_4 units invoking bending of the SiOSi bonds. As a matter of fact, it is possible to find support for this picture by simply comparing classical and quantum mechanical distribution functions of the SiO bond length and the SiOSi and OSiO bond angle distribution at room temperature, which is done in Figure 4. The quantum mechanical Si-O bond length deviates considerably from the classical bond length distribution, while the bending of both SiOSi and OSiO angle is still classical, i.e. low-energetic. The bending modes start freezing quantum mechanically at temperatures near 200 K, while the SiO bond length distribution remains essentially unaltered upon further cooling. Particularly strong quantum effects in distributions $p(r)$ or $p(\alpha)$ such as shown in Fig. 4 are found in cases where the crystal contains very light atoms, e.g. orthorhombic polyethylene C_nH_{2n+2} [Martonak et al. 1998].

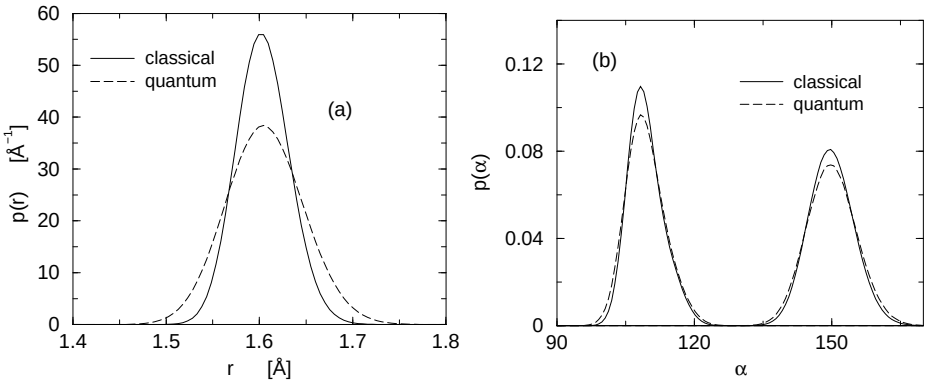

Figure 4: a) Probability density $p(r)$ to find an oxygen atom in a distance r from a silicon atom. b) O-Si-O (left) and Si-O-Si (right) bond angle distribution function $p(\alpha)$. Solid lines reflect classical simulations, dashed lines represent quantum mechanical simulations. Temperature $T = 300$ K. From Müser (2001).

4 The structure of β-quartz

The average structure of β quartz is hexagonal and the symmetry class is P622. However, the local structure is known to deviate considerably from the average structure and the nature of this deviation has been a subject of long debate. It was frequently discussed in reference to the nature of the α-β transition in quartz [Dolino 1990, Heaney, Prewitt, and Gibbs 1994, Carpenter et al. 1998]. The main issue is whether or not oxygen atoms oscillate around positions that correspond to locations on which oxygen atoms can be found in α quartz, so-called α_1 and α_2 positions. If β quartz consisted of small α_1 and α_2 domains (each occuring with the same probability), then the averaged structure would still be that of β quartz. Alternatively, one may envision a situation where the atoms oscillate around their β positions in such a way that the short-range order differs from that in α-quartz. Evidence for this was found by Kihara (1990), who suggested librational motion of the oxygen atoms around the Si-Si lines leading to non Gaussian atomic distribution functions.

In the following discussion, I will mostly disregard the intermediate incommensurate phase, which has been observed in a relatively small temperature range of 1.5 K [Dolino 1990] between the regions where α and β quartz are thermodynamically stable, respectively. The wavelength of the incommensurate soft mode exceeds the feasible linear dimension of our current atomistic simulation by more than an order of magnitude. Hence if we were to maintain the shape of our simulation box, we would have to deal with system sizes more than three orders of magnitude larger than those that are currently employed. Going to such large system sizes would be barely feasible at the present time on a clus-

ter containing a few workstations even with further simplifications of the model and optimization of the algorithm (replace Ewald sums with algorithms that are preferential for summing up Coulombic interactions of extremely large systems). One might argue that it could be sufficient to extend the size of the simulation cell parallel to the soft mode vector. However, this could change the effective dimensionality of our solid, which is likely to invoke a qualitatively different phase transition scenario. Note that studying relatively small systems of a few thousands of atoms is not necessarily a disadvantage. It has been argued that the α-β transition is first order due to the existence of the incommensurate phase in between the two phases. Our system sizes are too small to be affected by this intermediate phase, however, they are still large enough to determine the order of the transition via finite-size scaling.

I will first be concerned with a discussion of how to quantify and to observe the non-Gaussian behaviour of β quartz in atomistic computer simulations. One may expect that the behaviour is rather generic for network formers with tetrahedral short-range order and displacive phase transition between high symmetry (i.e. β-quartz) and low symmetry (i.e. α-quartz) phases. We will then explore the consequences that non-Gaussian behaviour has for quasi harmonic treatments. This will be done in Section 4.3. The relation of the local order in β-quartz with respect to that in α-quartz will be discussed in detail in Section 4.3.

4.1 Non-Gaussian disorder in β-quartz

Let us first discuss the information that is accessible to an experimentalist and explore possibilities how computer simulations can retrieve similar data or even go beyond. The key quantity in structure determination by elastic scattering (neutron or X-ray) is the scattering intensity $I(\mathbf{q})$

$$I(\mathbf{q}) = \sum_{ij} b_i b_j \left\langle \exp\left\{ i\mathbf{q}\left(\mathbf{R}_i - \mathbf{R}_j\right)\right\}\right\rangle , \tag{10}$$

with $\mathbf{q}$ the momentum transfer of the scattered neutron, b_i the cross section of atom i, and $\mathbf{R}_i$ its position in space. $\langle ... \rangle$ denotes a temporal average over a sample in thermal equilibrium. If the coupling between different vibrational modes in the crystal is weak, Eq. (10) can be simplified to

$$I(\mathbf{q}) = I_{\mathrm{ideal}}(\mathbf{q})\tilde{S}(\mathbf{q}), \tag{11}$$

where $I_{\mathrm{ideal}}(\mathbf{q})$ is the scattering intensity for the ideal structure (or average structure) and $\tilde{S}(\mathbf{q})$ is a weight factor, also known as Debye Waller factor, that depends on the amount of vibrational or structural disorder in the system. Unlike experiment, computer simulations can determine $I_{\mathrm{ideal}}(\mathbf{q})$ by first averaging the configurations over many time steps and then performing the scattering, i.e., the brackets $\langle ... \rangle$ are pulled into the argument of the exponential. Of course this

procedure is limited to time scales in which atomic diffusion within the solid can be neglected. Since in most solids the diffusive mechanisms take place on time scales distinctly larger than those accessible in molecular dynamics simulations, this effect can usually be neglected. Exceptions to this rule are quantum solids like crystalline helium and crystals near a (non-displacive) phase transition. In both cases significant diffusion can take place on the time scale of a MD simulation.

The dependence of $\tilde{S}(\mathbf{q})$ on q (the absolute value of $\mathbf{q}$) can be easily discussed in a one-dimensional system. This is done in Fig. 5 where the effect of phonons (Gaussian atomic distribution functions around the ideal positions) and disorder on the $\tilde{S}(\mathbf{q})$ is analyzed. The reader might consult standard solid state physics books in order to confirm the validity of the equations stated in that figure or derive them by using Eq. (10) and by decomposing the vibrations into harmonic eigenmodes. The main result for vibrational disorder is that the intensity of $I(q)$ is the product of the ideal scattering intensity $I_{\mathrm{ideal}}(q)$ times a weight function that falls off exponentially fast with the square of the scattered wave vector $\mathbf{q}$, while oscillation in $I(\mathbf{q})$ are indicative of structural disorder. Of course, the last row in Fig. 5 is highly idealized, because the atoms will oscillate around the split positions and because real crystals are not one-dimensional.

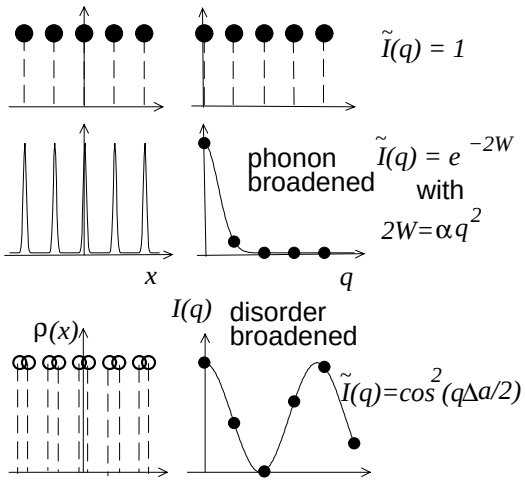

Figure 5: Schematic representation of the density distribution $\rho(x)$ in real space (left) and elastic scattering intensity $\tilde{I}(q)$ (right) for a one-dimensional one-component system. The top row represents the ideal/average structure, the middle row a phonon broadened structure, and the bottom row shows a disordered structure in which one (split) atom occupies randomly one out of two equivalent positions that are separated by Δa.

The qualitative discussion in Fig. 5 is also valid for solids with basis, i.e.

two-component systems like quartz. In order to generalize the analysis of how $\tilde{I}(\mathbf{q})$ depends on the inverse neutron wavelength $\mathbf{q}$, it is convenient to introduce the polarization vector $\mathbf{u}_{m\alpha}(\mathbf{Q})$ of the normal mode $(\mathbf{Q}, \alpha)$. The number of independent polarization vectors in a unit cell depends on the crystal symmetry.

In a computer simulation, we can restrict the evaluation of the scattering intensities, see Eq. (10), to pairs of atoms, which all have the same polarization vector $\mathbf{u}_{m\alpha}(\mathbf{Q})$ and $\mathbf{u}_{n\alpha}(\mathbf{Q})$, respectively. This enables us to define a generalized scattering intensities or generalized Debye-Waller factor $I_{mn}(\mathbf{q})$:

$$I_{mn}(\mathbf{q}) = \exp\left\{-q^2 \sum_{\mathbf{Q}\alpha} \langle [\mathbf{n}_{\mathbf{q}} \mathbf{u}_{m\alpha}(\mathbf{Q})] \, [\mathbf{n}_{\vec{q}} \mathbf{u}^*_{n\alpha}(\mathbf{Q})] \rangle \right\} . \tag{12}$$

While this generalized Debye-Waller factor is directly accessible in simulations, experimental determination of that quantity requires fitting and *a priori* assumptions on the atomic distributions. The $I_{mn}(\mathbf{q})$ have the important feature that they fall off according to $I \propto e^{-\alpha q^2}$ as long as the harmonic approximation is valid. The prefactor α in the exponential depends of course on the director $\mathbf{n}_{\mathbf{q}}$ of $\mathbf{q}$. The property $I \propto e^{\alpha q^2}$ is lost if the sum in Eq. (10) is evaluated over all atoms. The following example, see Fig. 6, shows how the calculation of I_{mm}'s can contribute to the determination of the local structure in β quartz.

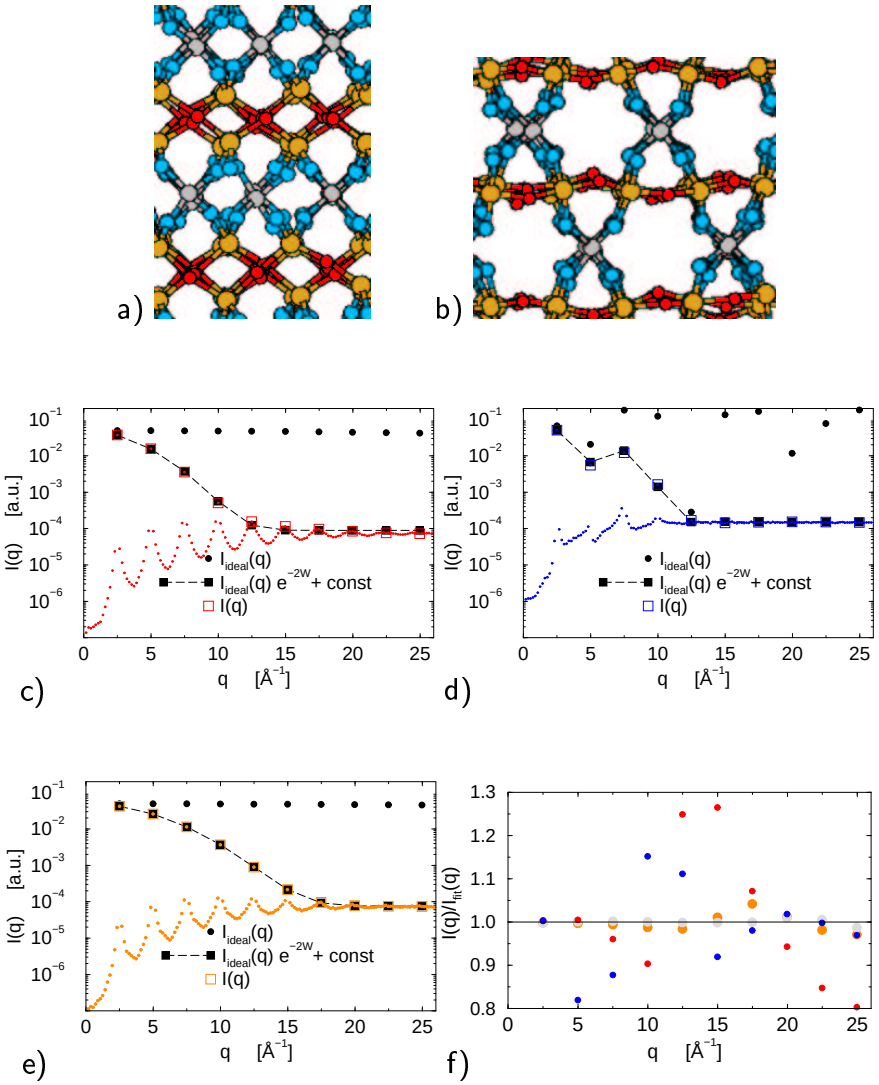

Figure 6: a) Snapshot of β quartz at $T = 1000$ K in the xz plane. x is horizontal. Ocher and grey colored atoms reflect Si atoms, red and blue show O atoms. b) Same as a) but for xy plane. c)-e) Generalized scattering intensities (ideal structure, real structure, and fits) as a function of q with $\mathbf{n}_q$ parallel to x axis. Colors are consistent with a) and b). The background in $I(q)$ [small circles in c)-e)] including the plateau value for large q becomes smaller with increasing system size. f) Observed scattering intensities $I(q)$ divided by fit values $I_{\rm fit}(q)$.

In Fig. 6, the (generalized) scattering intensities of the ideal sturcture (i.e. the structure averaged over a few 10,000 MD steps), the averaged scattering intensities I_{mm}, and fits are shown. The fits include an adjustable offset that is added to the Gaussian, i.e. $\tilde{I}_{\rm fit} = e^{-\alpha q^2} + \text{const}$. Only those $\mathbf{q}$ vectors are incorporated in the fit that correspond to "allowed" lattice vectors. The offset was observed to vanish with inverse particle number. The background at the symmetry forbidden q can be understood from the fact that the simulations were done in the isothermal-isobaric ensemble. One can see in Fig. 6 that the generalized scattering intensities $I_{mm}(\mathrm{q})$ are quite well described by the harmonic approximation if m denotes one of the two equivalent Si atoms. (The Si atoms are equivalent in the sense that they have the same polarization vector for an eigenmode $\mathbf{Q}, \alpha$.) The oxygen atoms show much larger deviations from harmonic behaviour than the silicon atoms, since the oxygen's $I_{mm}(q)$ can be fit considerably less well with Gaussians.

The non-Gaussian nature of the vibrations associated with the motion of oxygen atoms is also illustrated in Fig. 7, where the probability $p(r)$ to find an atom a distance r away from its average position (with respect to the center of mass of the simulation box) divided by r^2 is shown as a function of r. For the Si atoms, a single Gaussian is obtained, while the O atoms apparently have several preferred sites, which is obvious from the anomaly in the $p(r)/r^2$ curve. These results strongly support the X-ray study by Kihara (1990) in which the oxygen distribution functions were conjectured to deviate considerably from Gaussians.

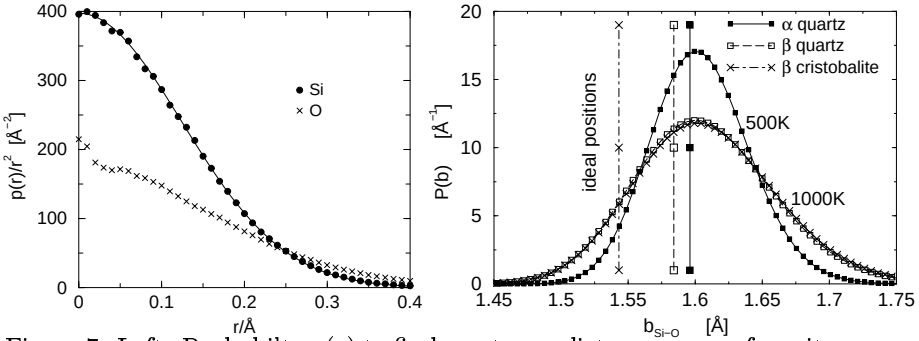

Figure 7: Left: Probabilty $p(r)$ to find an atom a distance r away from its average position (with respect to the center of mass of the simulation box) divided by r^2 as a function of r. Circles refer to Si atoms, crosses to O atoms. The straight line is a Gaussian fit through the Si data. $T = 900$ K. Right: Probabilty $p(b)$ to find an oxygen atom a distance b away from a silicon atom. β-quartz and β-cristobalite simulations were carried out at $T = 1000$ K, those for α-quartz at 500 K. The straight lines reflect the location of the Si-O bond lengths as deduced from the average structure. From Müser and Binder (2001).

Yet another indication for the fluctuations about the average positions being anharmonic is obtained from the bond-length distribution function. For

β-cristobalite, it has been shown experimentally that the real bond-length distribution function peaks at a radius that is distinctly larger than the bond-length deduced from the average structure [Dove et al. 1997]. This effect is less strong in β-quartz as shown in Fig. 7. Nevertheless it is clear that the tendencies in β-cristobalite and β-quartz are similar: The Si-O bond lengths deduced from the average structures is located at a position that is markedly smaller than the position where the bond length distribution peaks. The bond-lengths from the average positions shown in Fig. 7 are deduced from our simulations (see also Fig. 8). The values we obtain for β-cristobalite agree well with those suggested by Dove et al. (1997). They state that the bond length of the average position is about 1.55 Å, while their bond length distribution peaks at 1.61-1.62 Å. There is also qualitative agreement of our simulations with experimental data on β-quartz: Kihara (1990) reported a real SiO bond length of 1.62 Å, which is about 0.04 Å larger than the spectroscopic bond length of 1.588 Å, while our simulations suggest a change of only 0.02 Å. A recent neutron diffraction study confirms Kihara's results quite accurately [Tucker et al. 2000].

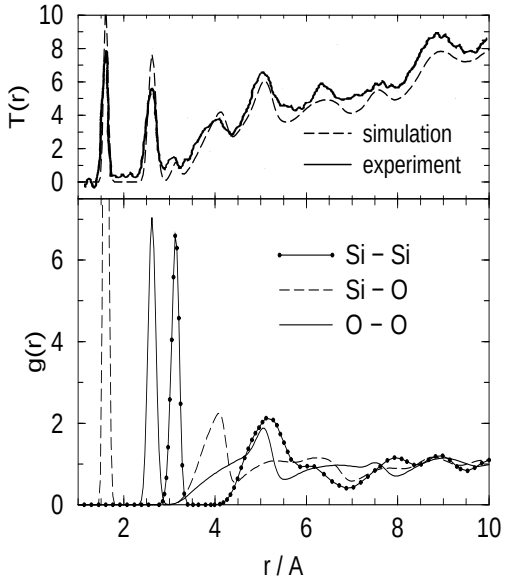

Figure 8: a) $T(r)$ for β-cristobalite as a function of distance r at 573 K. Experiment is represented by a solid line and simulation data is represented by a dashed line. b) Corresponding radial distribution function $g(r)$ for Si-Si, Si-O, and O-O bonds. The curves are normalized such that $g(r) \to 1$ for $r \to \infty$. From Rickwardt et al. (2001).

While we are mainly concerned with β-quartz in this chapter, it should not remained unmentioned that simulations based on the BKS potential yield ex-

cellent agreement for the instantaneous order in other polymorphs as well, i.e. β-cristobalite. It is a cubic SiO_2 polymorph in which the Si are four fold coordinated like in quartz. Information on the instantaneous order can be obtained experimentally by measuring the so-called total pair correlation function $T(r)$. This function is a sum of SiSi, SiO, and OO pair correlation function $g(r)$, whereby each function is weighted with the cross section b of the atoms involved, hence for SiO_2:

$$T(r) \propto b_{\mathrm{Si}} b_{\mathrm{Si}} g_{\mathrm{SiSi}}(r) + 2 b_{\mathrm{Si}} b_{\mathrm{O}} g_{\mathrm{SiO}}(r) + 4 b_{\mathrm{O}} b_{\mathrm{O}} g_{\mathrm{SiO}}(r). \tag{13}$$

I refer to Ref. [Dove et al. 1997] for technical details on how to obtain $T(r)$ experimentally. Again, the simulations provide a unique way to determine the individual $g(r)$'s directly whithout any assumptions on the structure or any kind of *a priori* assumptions. The results for $T(r)$ as obtained for β-cristobalite are shown in Fig. (8a) while the radial distribution functions are displayd in Fig. (8b). It is interesting to note that the peak in $T(r)$ at about $5\,\mathring{A}$ is due to a simultaneous maximum in $g_{\mathrm{OO}}(r)$ and $g_{\mathrm{SiO}}(r)$, while the peak in $T(r)$ at $6.25\,\mathring{A}$ does not have a corresponding peak in any $g(r)$. The large local maximum in $T(r)$ at about $9\,\mathring{A}$ is then located at a position where all $g(r)$'s have a local maximum as well. The shape of $T(r)$ is particularly sensitive to details of the potentials at large distances, e.g., cutting off the short-range part of the potential at $4.5\,\mathring{A}$ alters $T(r)$ significantly for $r \geq 8\,\mathring{A}$.

4.2 Implications for quasi-harmonic treatments

Here, I want to argue that the seemingly small deviation from harmonic behaviour - as seen in the previous subsection - has dramatical consequences for quasi-harmonic treatments of the high-temperature phase of quartz. Of course, one may also expect similar difficulties with other high-temperature phases of network formers with similar tetrahedral short-range order. Quasi-harmonic approximations are done by expanding the potential energy surface about the experimentally observed ideal reference structure. From the bond length distribution one can see that this reference structure is not the most likely structure and hence the outlined expansion risks to fail in providing reliable structural and elastical properties.

Table 1 contains the list of various structural and elastic properties of α quartz and β quartz at temperatures $T = 300$ K and $T = 1000$ K, respectively. I compare experiments with molecular dynamics simulations carried out at finite temperatures and include data as obtained from harmonic approximations. The results for the harmonic approximations contain a treatment in which the BKS potential is used and lattice constants and elastic moduli are evaluated under the constraints that the silicon atoms remain on ideal β-quartz lattice position. The oxygen atoms were allowed to move freely, i.e. to relax to their ideal lattice positions and fluctuate around them. This procedure is strongly related to the

	exper.[a]	MD[b]	BKS (h)[c]	*ab-initio*[d]
a(300 K)	4.914	4.967	4.941	4.899
a(1000 K)	5.000	5.031	5.022	5.026
$100\Delta a/a$	1.72	1.29	1.62	2.59
c(300 K)	5.406	5.470	5.449	5.383
c(1000 K)	5.459	5.528	5.538	5.512
$100\Delta c/c$	0.98	1.06	1.65	2.39
C_{11}(300 K)	086.4	087.1	090.5	
C_{11}(1000 K)	132.2	140.6	266.0	
$\Delta C_{11}/C_{11}$	0.53	0.61	1.96	
C_{33}(300 K)	103.9	101.2	107.0	
C_{33}(1000 K)	121.4	127.5	227.0	
$\Delta C_{33}/C_{33}$	0.17	0.26	1.12	
B_0(300 K)	038.1	036.3	040.5	035.4
B_0(1000 K)	070.2	079.8	164.0	132.6
$\Delta B_0/B_0$	0.84	1.20	3.10	3.75

Table 1: Lattice constants a and c in α quartz (T = 300 K) and β-quartz (T = 1000 K), along with some representative elastic moduli. Differences between values of a, c, or C_{ij} between the α and the β phase are inserted as well. [a] Carpenter et al. (1998) (experiments), [b] Müser and Binder (2001) (finite T simulations), [c] van Beest, Kramer, and van Santen (1990) (in harmonic approximation, data for T = 1000 K unpublished results from present author), [d] Demuth et al. (1999) (local density approximation, harmonic approximation).

way in which the elastic constants (and lattice parameters) are obtained in a local density approximation (LDA) calculation by Demuth et al. (1999) whose results are inserted as well for comparison.

It can be seen that structural parameters and elastic constants are in good agreement for the low-temperature phase in all cases. This speaks in favor for both the BKS potential and the LDA calculation by Demuth et al. In the high-temperature phase, however, only the molecular dynamics simulations that implicitly include the non-Gaussian lattice deformations agree satisfactorily with experiment while both harmonic treatments predict a bulk modulus which is about a factor two too large. Unfortunately no data was provided by Demuth et al. (1999) on other elastic properties. The disagreement between harmonic treatments and experiment is even worse if one looks at the difference between high and low temperature phases.

Since the BKS potential agrees well with experiment when all thermal fluctuation are taken into account via MD simulations and the trend in the harmonic approximation of BKS and *ab initio* are similar, it seems that Demuth et al.'s

LDA treatment is quite reasonable and one should acknowledge the fact that these data were made public, albeit the discrepancy between calculations and experiments were pointed out by the authors themselves.

Yet, the message to be learned is that elastic properties and changes in the lattice parameters can not be obtained from regular *ab initio* calculations in a high-temperature polymorph if the atomic probability distribution functions deviate from Gaussians in a way is similar to the deviation seen in β-quartz. Of course Car-Parrinello type simulations allow the determination of all these properties provided that the simulations cells are sufficiently large and the statistics sufficiently good. In the present case, we needed a few 10,000 MD steps and a little less than thousand atoms in order to get elastic constants with an accuracy of about 5 percent accuracy.) While elastic constants can be evaluated much faster in the NVT ensemble than in the NpT ensemble at small temperatures, this statement becomes incorrect in the high-temperature phase, because the thermal fluctuation corrections are in the order of the harmonic constants evaluated in the harmonic approximation. Since time steps are considerably smaller in Car-Parrinello simulations and since each individual time step is much more CPU time expensive, it seems that classical (or path integral) molecular dynamics are the only reliable route to do these calculation for the next few years.

4.3 Nature of the α-β phase transition

In the previous discussion, we have only learned that the disorder is non-Gaussian, but nothing has been said to the nature of the disorder. If β-quartz consisted of α_1 and α_2 domains, which spatially and dynamically averaged to the idealized β-quartz structure, then the phase transformation could be expected to be an order-disorder transition. Neutron diffraction [Wright and Lehman 1981], NMR studies [Spearing et al. 1992], and molecular-dynamics simulations [Tsuneyuki et al. 1990] were interpreted as evidence for this scenario. The majority of recent studies, however, favors a displacive type of phase transformation. In this case, the actual structure of the high-temperature phase is interpreted as an ideal β-quartz structure, which is distorted by rigid unit modes of relatively stiff tetrahedral SiO_4 units. This point of view explains the existence of soft modes in the α and β phases [Axe and Shirane 1970, Tezuka et al. 1991, Carpenter et al. 1998, Dove et al. 1999] and the absence of symmetry forbidden phonons in the β-phase of quartz [Salje et al. 1992]. The non Gaussian behaviour observed by Kihara (1990) mentioned above favored an ordered structure. The non Gaussian behaviour was not interpreted as disorder but as librational motion of the oxygen atoms around the Si-Si lines.

In order to gain insight into the local structure, it is convenient to calculate radial distribution functions $g_{\mathrm{SiSi}}(r)$, $g_{\mathrm{SiO}}(r)$, and $g_{\mathrm{OO}}(r)$. As mentioned above, all these three radial distribution functions can be obtained individually in a straightforward way and with very good accuracy, and thus complement experiments where this information is not easily available. The $g(r)$'s are shown in

Fig. 9 a little more than 100 K above and below "our" phase transition temperature of $T_{\rm tr} = 740\,{\rm K} \pm 5\,{\rm K}$. (The determination of $T_{\rm tr}$ will be outlined below.) It can be seen that most features are similar in the two phases even for relatively large distances r. This raises the question whether or not one can interpret the $g(r)$'s as measured in β-quartz as a mere temperature broadened version of the α-quartz configuration. If this was the case the picture of the domain disorder in β-quartz would be supported. If it is possible to find qualitative features in $g(r)$ in β quartz that are not akin of those in α quartz (in particular for small r), then the domain picture can be ruled out.

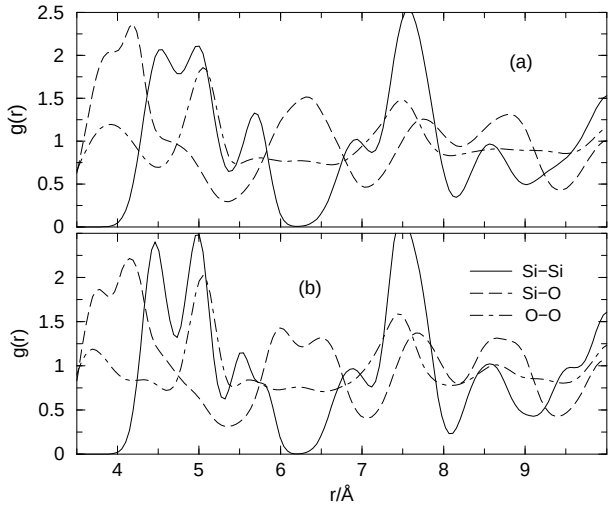

Figure 9: Radial distribution functions for $3.5\,\mathring{A} < r < 10.0\,\mathring{A}$ at temperatures (a) $T = 875$ K (α-quartz) and (b) $T = 625$ K (β-quartz). From Müser and Binder (2001).

In order to investigate this issue in more detail, it is best to calculate the various $g(r)$'s at a temperature where both phases are thermodynamically stable or at least metastable, i.e. in the immediate vicinity of $T_{\rm tr}$. It turns out that all $g(r)$'s evolve rather smoothly in either phase, however, there is a sudden change by going from the α phase to the β phase. This behaviour is illustrated in Fig. 10 for selected areas of various $g(r)$'s. The configurations in Fig. 10 at $T = 750$ K have been equilibrated for 3000 MD steps before the radial distribution functions were averaged over 2000 MD steps. The initial configurations were equilibrated configurations from 25 K below or above 750 K. Smaller systems, e.g., $N = 1080$ systems relax considerably at $T = 750$ K within the above mentioned equilibration time period. One β quartz configuration was quenched down to $T = 10$ K in order to find the inherent structure of a typical β-quartz configuration. Quenching is done by suddenly dropping the temperature and

chosing much larger couplings to the thermostat than usual.

Fig. 10 reveals that the local structures in β-quartz can certainly not be interpreted as (temperature) broadened α-quartz domains, e.g., there are clear double peaks in g_{SiSi} at $r \approx 5.6$ Å and g_{SiO} at $r \approx 6.25$ Åin the α phase that are absent in the β phase. The various $g(r)$'s do not change significantly with temperature above T_{tr}, but make sudden changes near and below T_{tr}. The (double) peaks in $g(r)$ become increasingly more pronounced as the temperature is lowered further below T_{tr}. This is furthermore supported by the striking observation that no double peak in the SiSi radial distribution function is observed when $T = 750$ K configurations are quenched down to $T = 10$ K (Fig. 10d). These findings support an experimental study by Tucker et al. (2000), who deduced the nearest-neighbor Si-Si-Si angle distribution from the so-called total pair correlation function $T(r)$. They found that two peaks of the Si-Si-Si angle distribution coalesced upon heating at the $\alpha - \beta$ phase transition.

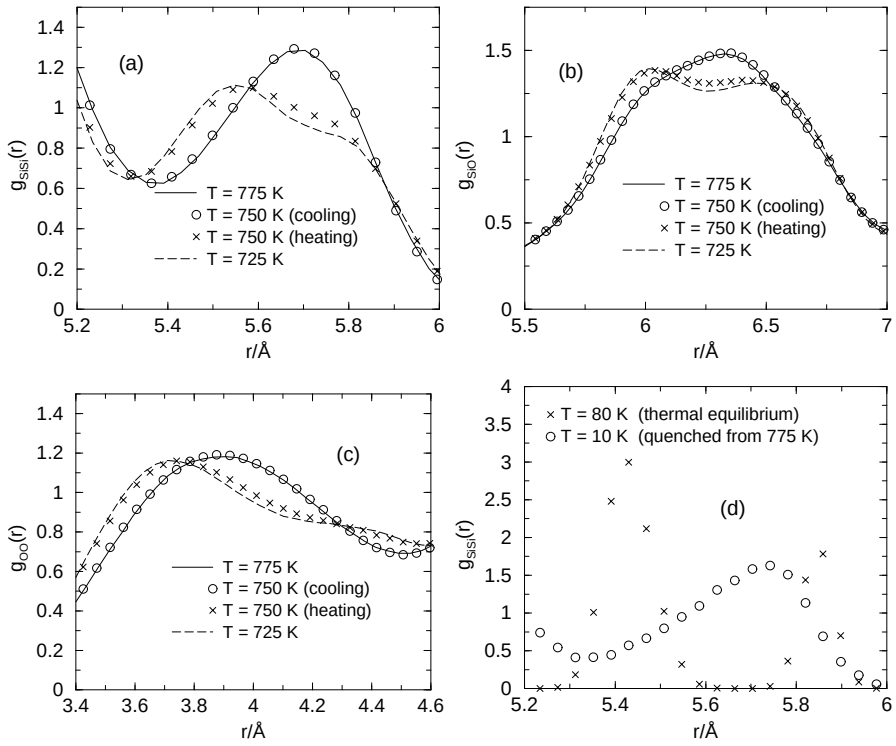

Figure 10: Details of the radial distribution function Si-Si (a), Si-O (b), and O-O (c) for system size $N = 4320$ at various temperatures. (d) is same as (a), but from configurations that have been quenched from high temperature phase to 10 K.

In order to analyze the α-β transition in more detail, it is instructive to visualize the changes of the structure in quartz. This is done in Fig. 11, where a snapshot along the [100] axis is taken for α-quartz at $T = 80$ K and for β-quartz at $T = 1050$ K. The rotation of tetrahedra about the [100] axis can be seen particularly well for the positions that are equivalent to those sites marked by an arrow. In the β-quartz phase, no α_1 or α_2 domains become apparent. This statement also holds for most configurations obtained near but above $T_{\rm tr}$. For large system sizes near $T_{\rm tr}$, it is actually possible to observe jumps of the entire system between configurations that entirely resemble the α-quartz structure and those that resemble β-quartz.

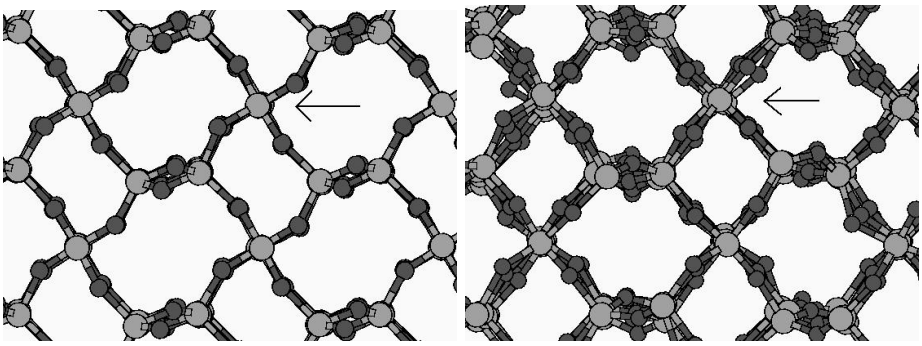

Figure 11: View along the [100] axis in α-quartz at $T = 80$ K (left) and β-quartz at $T = 1050$ K (right). Dark and light atoms represent oxygen and silicon atoms respectively. Both snapshots belong to identical subvolumes of the simulation cell. The [001] axis goes from the left to the right. The rotation angles about the [100] axis of the units marked by an arrow is used to define the order parameter. From Müser and Binder (2001).

In order to obtain information about the order in the system, a global order parameter ϕ is defined that measures the rotation of (distorted) tetrahedra about the [100] axis, such that

$$\phi = \frac{1}{N^*} \sum_{i^*=1}^{N^*} \varphi_{i^*}, \tag{14}$$

where the sum over i^* is confined to sites which are equivalent to the sites marked by an arrow in Fig. 11. φ_i^* denotes the (averaged) deviation of the orientation in the y-z plane of the (four) Si-O bond(s) from the value in the ideal β-quartz structure.

The sudden structural change in the local structure indicates that the transition is of first order. Yet a proper finite-size scaling analysis has to be done in order to make this sure [Binder and Stauffer 1987]. Such a study could address the speculation whether the first-order nature of the transition merely arises due to the incommensurate instability that occurs at a temperature which is 1.5 K

higher than the transition into the α phase. As argued above the incommensurate phase will be strongly suppressed in simulations owing to the large gap between the linear box dimension in our simulation and the length of the wave length of the incommensurate mode.

It is difficult to locate $T_{\rm tr}$ precisely by just calculating the expectation value of the (absolute value) of ϕ, because all thermodynamic properties behave smoothly for finite-size systems near the phase transition temperature. In order to determine the transition temperature $T_{\rm tr}$ nevertheless accurately, use is made of the fourth' order cumulant [Binder 1981], which is defined in the case of a one-component order parameter as

$$g_4(N,T) = \frac{1}{2}\left(3 - \frac{\langle\phi^4\rangle_N}{\langle\phi^2\rangle_N^2}\right), \tag{15}$$

where $\langle\phi^k\rangle_N$ denotes the thermal average of the k'th moment of the order parameter for an N-particle system. It has been shown [Vollmayr et al. 1993] that $g_4(N,T)$, aside from small correction terms, has a size-independent crossing point g_4^* at a first-order phase transition. For the calculation of g_4^*, the geometry of the simulation cell is supposed to be constant. It is difficult to satisfy this requirement without increasing the particle number N considerably for the quartz structure if the cell geometries are approximately cubic. The smallest box length should exceed twice the cutoff radius which limits us to $N \geq 1080$. While it is still possible to equilibrate system sizes of the order $N \approx 2000$ near the phase transition, this becomes extremely difficult for $N \approx 4000$. Note that the equilibration time increases algebraicly with N at a second-order and exponentially with N at a first-order transition point.

The expectation values of the cumulants are shown in Fig. 12. Due to the fact that the cell geometry slightly differ between the $N = 1080$ and the $N = 2160$ system, we can not expect perfect crossing of the two different systems at $T_{\rm tr}$. However, comparison to the value where the cumulants cross in a Landau description of this transition (see below for more details) makes it plausible that the crossing of the cumulants shown in Fig. 12 is indeed meaningful. Within the statistical error bars, it is possible to locate the transition at $T_{\rm tr} \approx 740$ K with an uncertainty of about 5 K for both system sizes.

In order to describe the transition within a Landau theory with a single scalar order parameter, we adopt the form [Carpenter et al. 1998]

$$F(\phi,T) = \frac{1}{2}a(T - T_{\rm c})\phi^2 + \frac{1}{4}b\phi^4 + \frac{1}{6}c\phi^6, \tag{16}$$

where F is the free-energy per particle as a function of temperature T and order parameter ϕ while a, b, c, and $T_{\rm c}$ are (free) parameters. In order to find those parameters that are appropriate to describe our simulation results, we need to generalize the approach to *finite* system sizes. This is done by evaluating numerically expectation values of the n'th power of ϕ using ($\beta = 1/k_BT$) in the

following way:

$$\langle \phi^n \rangle = \frac{\int_{-\infty}^{\infty} d\phi \, \phi^n \, \exp\{-\beta N F(\phi, T)\}}{\int_{-\infty}^{\infty} d\phi \exp\{-\beta N F(\phi, T)\}}. \tag{17}$$

The parameters a, b, c, and T_c were determined by fitting the temperature dependence of the order parameter $\langle \mid \phi \mid \rangle$ for the $N = 1080$ system. The fit is shown on the right-hand side of Fig. 12 along with similar data for $N = 2160$. We also included data in which the thermodynamic limit was taken. It can be seen that the size effect in $\langle \mid \phi \mid \rangle$ is reasonably described by Landau theory.

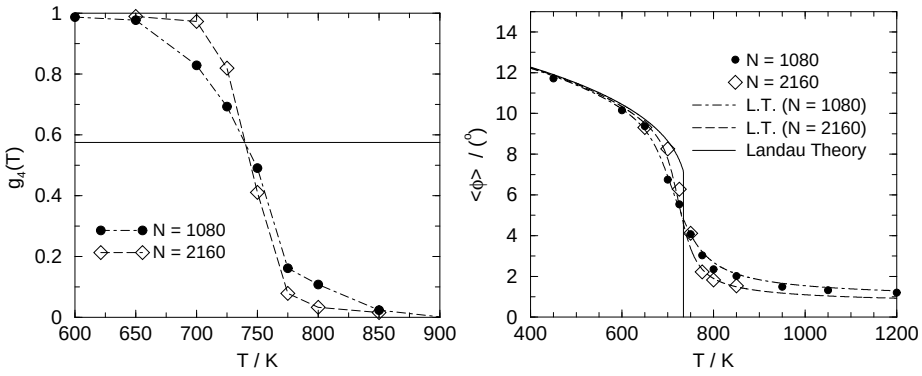

Figure 12: Left: Fourth order cumulant g_4 as a function of temperature T for two different system sizes. The value g_4^* at which crossing of the cumulants is predicted within Landau theory is indicated by a straight line. Broken lines are drawn to guide the eye. Right: Order parameter $\langle \mid \phi \mid \rangle$ as a function of temperature. The lines reflect fits according to Landau theory, whose free parameters were adjusted to the $N = 1080$ curve. The solid line corresponds to the thermodynamic limit in Landau theory, Broken lines represent finite-size Landau theory. From Müser and Binder (2001).

Overall, similar coefficients as from experimental data are drawn from the simulations. Most importantly, the parameter b is found to be slightly negative, $T_c = 715$ K is obtained about 115 K smaller than in experiment, and $T_t - T_c \approx 20\,K$ is found about twice as large as in real experiment [Carpenter et al. 1998]. Nonetheless, the global picture of experiment is certainly reproduced. Since lattice parameters, elastic constants, and phase transition agree reasonably well with experiment, it is safe to draw qualitative conclusions about properties which are easily accessible in the simulation, but not as easily accessible experimentally, i.e., information on the local structure.

5 Mechanical stability of quartz-I and quartz-II

In this section, we will be concerned with another phase of quartz, namely the high-pressure phase called quartz II. Quartz II is a silica polymorph that can be obtained from α-quartz by slowly increasing the external pressure P to values slightly larger than $P_{\mathrm{I-II}} = 21$ GPa [Kingma et al. 1993]. The crystal-crystal transition has been observed a little less than a decade ago and the mechanism driving the transition is still subject of a controversial debate [Binggeli and Chelikowsky 1992, Gregoryanz et al. 2000, Müser and Schöffel 2001]. Computer simulations of regular quartz (quartz I) suggested that one of the Born stability criteria (BSC) was expected to be violated in α-quartz at 25 GPa and the transition from quartz I to quartz II was related to this mechanical instability [Binggeli and Chelikowsky 1992]. A reanalysis of the BSC in terms of experimentally measured elastic constants, however, found a large discrepancy to these theoretical predictions [Gregoryanz et al. 2000]: The hypothetical, mechanically (meta)stable pressure regime of quartz I for $P > P_{\mathrm{I-II}}$ was found to go up to values as large as 40 GPa. Snapshot of the pressure induced phase transformation are shown in Fig. 13

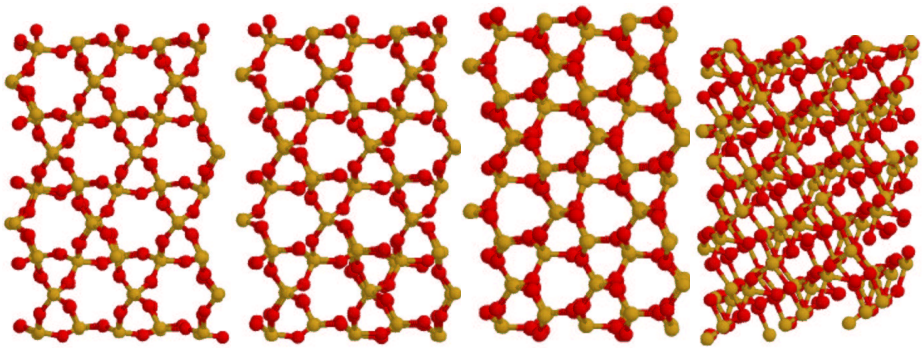

Figure 13: Snapshot of quartz under pressures at: $p = 0$, 8, 21, and 22 GPa (from the left to the right).

The suspicion has been raised that this discrepancy might be due to an inconsistent evaluation of the BSC [Müser and Schöffel 2001]: The definition of second-order elastic constants is not unique at non-zero pressures. It is commonly distinguished between elastic constants C_{ij} and stiffness or Birch coefficients B_{ij} [Wallace 1971]. The latter are obtained from evaluating Eq. (7), while the C_{ij} are obtained by using the standard estimators for elastic constants in the NVT ensemble. The proper BSC for non-zero pressures is to require that the matrix B_{ij} be positive definite [Wang et al. 1993]. Thus, when analyzing the mechanical stability of α-quartz under pressure, the BSC

$$B_3 = (C_{11} - C_{12})C_{44} - 2C_{14}^2 > 0 \tag{18}$$

is not meaningful. This condition has often been examined when discussing whether the pressure induced amorphization transition reported in molecular dynamics simulations (MDS) is driven by a mechanical instability [Gregoryanz et al. 2000, Binggeli and Chelikowsky 1992, Tse, Klug and Le Page 1992].

Distinguishing between Birch and elastic constants reveals that the BSC overestimates the stability of α-quartz under pressure considerably. This is shown in Fig. 14. In the inset of that figure it can be seen that the MDS reproduce the experimentally measured pressure dependence of B_3 fairly well. This comparison justifies the use of the emploied model potential surface for the stability analysis. If $B_{\alpha\beta}$ replace $C_{\alpha\beta}$ in Eq. (18) the behavior is similar to the one reported by Binggeli and Chelikowsky [Binggeli and Chelikowsky 1992], e.g., a zero slope of B_3 at small pressures is found.

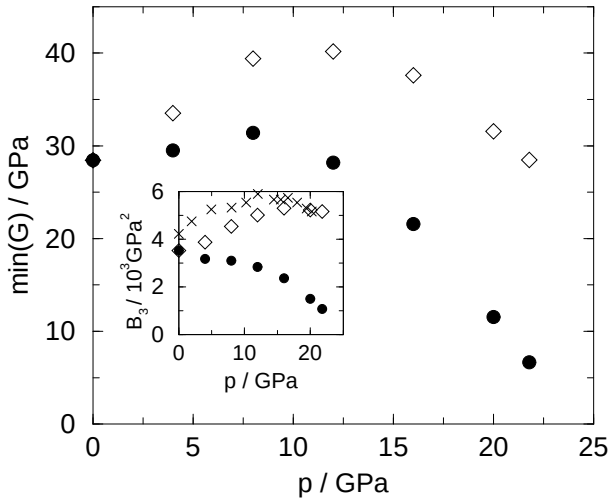

Figure 14: Minimum eigenvalue of the matrix of the elastic constant (open diamonds) and of the Birch matrix (filled circles) as a function of pressure. Inset: Born stability criterion applied to elastic constants (diamonds) and Birch coefficients (closed circles). Error bars are about symbol size. Crosses represent data from Gregoryanz et al. (2000).

The correct stability criterion is examined in the main part of Fig. 14. The smallest eigenvalue of the Birch coefficients tends to zero much faster than the stability criterion (using regular elastic constants) related to Eq. (18). From the main part of Fig. 14, mechanical instability would be expected at a pressure $p \approx 25$ GPa, while the former analysis predicts an instability at $p \approx 40$ GPa.

Preliminary analysis shows that the transition between α-quartz and quartz II is kinetically hindered and non-reversible, but these studies will only be published in the near future.

6 Conclusions

These lecture notes gave an overview over selected computer simulation studies of the structure of β-quartz, the temperature driven phase transition between β-quartz and α-quartz and the pressure driven phase transition between α-quartz and quartz II. The relationship between structure and structure fluctuations on one hand and elastic properties and phase transition driving mechanisms on the other hand was explored. Some features turned out to be more complex than those that we know from one-component systems, i.e., the non-Gaussian nature of the local disorder in β-quartz and the consequences for the harmonic properties. Many conclusions drawn here can be believed to be rather generic for solids with similar tetrahedral local order (cristobalite, various phases of GeO_2, etc.).

It was also shown how model potentials for relatively complex systems can be tested in computer simulations. This is done by evaluating lattice parameters, elastic constants, and thermal expansion at low temperature. In the latter case, quantum effects of the ionic motion need to be taken into account. It was also shown that the use of finite-size scaling techniques, which are usually only applied to models (that are computationally much more feasible, Ising model, simple Lennard-Jonesium, etc.) is perfectly adequate to analyze phase transitions in more complex materials.

Acknowledgments. We are grateful for financial support for this research from the Materialwissenschaftliches Forschungszentrum (MWFZ) Mainz, the Bildungsministerium Für Bildung und Forschung (BMBF) in the framework of the Kompetenzzentrum 'Werkstoffsimulation' (grant N^o 03N6015) and from Schott Glaswerke. The author thanks K. Binder for useful discussions.

References

[Allen and Tildesley 1987] Allen M. P. and Tildesley D. J. (1987) Computer Simulations of Liquids. (Clarendon Press, Oxford).

[Axe and Shirane 1970] Axe J. C. and Shirane G. (1970) Study of the α-β phase transformation by inelastic bneutron scattering. Phys Rev. B 1: 342-348.

[Barker 1979] Barker J. A. (1979) A quantum-statistical Monte Carlo method; path integrals with boundary conditions, J. Chem. Phys. 70, 2914-2918.

[Binder 1981] Binder K. (1981) Critical properties from Monte Carlo: Coarse graining and renormalization. Phys. Rev. Lett. 47: 693-696.

[Binder and Stauffer 1987] Binder K. and Stauffer D. (1987) in *Applications of the Monte Carlo Method in Statistical Physics*, edited by K. Binder (Springer, Berlin)

[Binggeli and Chelikowsky 1992] Binggeli N. and Chelikowsky J. R. (1992) Elastic instability in α-quartz under pressure. Phys. Rev. Lett. 69, 2220-2223.

[Carpenter et al. 1998] Carpenter MA, Salje EKH, Graeme-Barber A, Wrucki B, Dove MT, and Knight KS (1998) Calibration of excess thermodynamic properties and elastic constant variations associated with the $\alpha \leftrightarrow \beta$ phase transition in quartz. Am. Mineral. 83: 2-22.

[Demuth et al. 1999] Demuth T., Jeanvoine Y., Hafner J., and Angyan J. G. (1999) Polymorphism in silica studied in the local density and generalized-gradient approximation. J. Phys.: Condens. Matter 11: 3833-3874.

[Dolino 1990] Dolino G. (1990) The α-inc-β phase transition of quartz: A century of research on displacive phase transitions. Phase Transitions 21: 59-72.

[Dove et al. 1997] Dove M. T., Kreen D. A., Hannon A. C., and Swainson IP (1997) Direct measurement of the Si-O bond length and orientational disorder in the high-temperature phase of cristobalite. Phys. Chem. Minerals 24: 311-317.

[Dove et al. 1999] Dove M. T., Gambhir M., Heine V. (1999) Anatomy of a structural phase transition: theoretical analysis of the displacive phase transition in quartz and other silicates. Phys. Chem. Minerals 26: 344-353.

[Feynman and Hibbs 1965] Feynman R. P. and Hibbs A. R. (1965) *Quantum Mechanics and Path Integrals.* (Mc.Graw-Hill, New York).

[Frenkel and Smit 1996] Frenkel D. and Smit B. (1996) Understanding Molecular Simulation: From Algorithms to Applications. (Academic Press, San Diego).

[Gregoryanz et al. 2000] Gregoryanz E., Hemley R. J., Mao H. K., Gillet P. (2000) High-pressure elasticity of α-quartz: Instability and ferroelastic transition. Phys. Rev. Lett. 84: 3117-3120.

[Heaney, Prewitt, and Gibbs 1994] Heaney P. J., Prewitt C. T., and Gibbs G. V. (Eds.) (1994) Silica. Physical behavior, geochemistry, and materials applications. (Mineralogical Society of America, Washington, D.C.).

[Kihara 1990] Kihara K. (1990) An X-ray study of the temperature dependence of the quartz structure. Eur. J. Mineral. 2: 63-77.

[Kingma et al. 1993] Kingma K. J., Hemley R. J., Mao H. K., and Veblen D. R. (1993) New high-pressure transformation in α-quartz. Phys. Rev. Lett. 70, 3927-3930.

[Landau and Binder 2000] Landau D.P. and Binder K. (2000) A guide to Monte Carlo simulations in statistical physics. (Cambridge University Press, Cambridge)

[Martonak et al. 1998] Martonak R., Paul W., and Binder K. (1998) Orthorhombic phase of crystalline polyethylene: A constant pressure path-integral Monte Carlo study. Phys. Rev. E 57, 2425-2437 (1998).

[Müser et al. 1995] Müser M. H., P. Nielaba, and K. Binder (1995) Path-integral Monte Carlo of crystalline Lennard-Jones systems, Phys. Rev. B 51, 2723-2731 (1995).

[Müser 2001] Müser M. H. (2001) Simulation of material properties below the Debye temperature: A path-integral molecular dynamics case study of quartz. J. Chem. Phys. 114, 6364-6370.

[Müser and Binder 2001] Müser M. H. and Binder K. (2001) Molecular dynamics study of the α-β transition in quartz: Elastic properties, finite size effects, and hysteresis in the local structure. Phys. Chem. Min. **28**, 746-755.

[Müser and Schöffel 2001] Müser M. H. and Schöffel P. (2001) Comment on: High-pressure elasticity of α-quartz: Instability and ferroelastic transition. cond-mat/0009353.

[Parrinello and Rahman 1980] Parrinello M. and Rahman A. (1980) Crystal structure and pair potentials: A molecular-dynamics study. Phys. Rev. Lett. **45**, 1196-1199.

[Parrinello and Rahman 1981] Parrinello M. and Rahman A. (1981) Polymorphic transitions in single crystals: A new molecular dynamics method. J. Appl. Phys. 52, 7182-7190.

[Parrinello and Rahman 1982] Parrinello M. and Rahman A. (1982) Strain fluctuations and elastic constants. J. Chem. Phys. **76**, 2662-2666.

[Rickwardt et al. 2001] Rickwardt Chr., Nielaba P., Müser, and Binder K. (2001) Path integral Monte Carlo simulation of silicates. Phys. Rev. B 63, 045204 (2001).

[Salje et al. 1992] Salje E. K. H., Ridgwell A., Güttler B., Wruck B., Dove M. T., and Dolino G. (1992). On the displacive character of the phase transition in quartz: A hard mode spectroscopic study. J. Phys.: Condens. Matter 4: 571-577.

[Schneider and Stoll 1978] Schneider T. and Stoll E. (1978) Molecular dynamics study of a three-dimensional one-component model for distortive phase transitions. Phys. Rev. B 17, 1302-1322.

[Schöffel and Müser 2001] Schöffel P. and Müser M. H. (2001), Elastic constants of quantum solids by path integral simulations, Phys. Rev. B 63 (22), 4108-1 - 4108-9.

[Spearing et al. 1992] Spearing D. R., Farnan I., and Stebbins J. F. (1992) Dynamics of the α-β transition in quartz and cristobalite as observed by in-situ high temperature ^{29}Si and ^{17}O NMR. Phys. Chem. Min. 19: 307-321.

[Striefler and Barsch 1975] Striefler M. E. and G. R. Barsch G. R., Phys. Rev. B **12**, 4553 (1975).

[Tezuka et al. 1991] Tezuka Y., Shin S., and Ishigame M. (1991) Observation of the silent soft phonon in β-quartz by means of hyper-Raman scattering. Phys. Rev. Lett. 66: 2356-2359.

[Tse and Klug 1991] Tse J. S. and Klug D. D. (1991) The structure and dynamics of silica polymorphs using a two-body effective potential. J. Chem. Phys. 95, 9176-9185.

[Tse, Klug and Le Page (1992)] Tse J. S., Klug D. D., and Y. Le Page Y. (1992) High-pressure densification of amorphous silica. Phys. Rev. Lett. **69**, 3647.

[Tsuneyuki et al. 1988] Tsuneyuki S., Tsukada M., Aoki H., and Matsui Y. (1988) First principles interatomic potential of silica applied to molecular dynamics. Phys. Rev. Lett. 61: 869-872.

[Tsuneyuki et al. 1990] Tsuneyuki S., Aoki H., and Tsukada M., (1990) Molecular-dynamics study of the α to β structural phase transition in quartz. Phys. Rev. Lett. 64: 776-779.

[Tucker et al. 2000] Tucker M. G., Dove M. T., Keen, D. A. (2000) Simultaneous analysis of changes in long-range and short-range structural order at the displacive phase transition in quartz. J. Phys.: Condens. Matter 12: L723-L730.

[Tuckerman et al. 1993] Tuckermann M. E., Berne B. J., Martyna G. J., and Klein M. L. (1993) Efficient molecular dynamics and hybrid Monte Carlo algorithms for path integrals. J. Chem. Phys. 99, 2796-2808.

[van Beest, Kramer, and van Santen 1990] van Beest B., Kramer G., and van Santen (1990) Force fields for silicas and aluminophosphates based on ab initio calculations. Phys. Rev. Lett. 64, 1955-1958.

[Vollmayr et al. 1993] Vollmayr K., Reger J. D., Scheucher M., and Binder K. (1993) Finite size effects at thermally-driven first order phase transitions: A phenomenological theory of the order parameter distribution. Z. Phys. B 91: 113.

[Wallace 1971] Wallace D. C., in *Solid State Physics* **25**, ed. H. Ehrenreich, F. Seitz, and D. Turnbull (Academic Press, New York, 1971); *Thermodynamics of Crystals* (Wiley, New York, 1972).

[Wang et al. 1993] Wang J.,Yip S.,Phillpot S. R., and Wolf D. (1993) Crystal instabilities at finite strain. Phys. Rev. Lett. **71**, 4182-4185.

[Wright and Lehman 1981] Wright A. F. and Lehmann M. S. (1981) The structure of quartz at 25 and 590^{o}C determined by neutron diffraction. J. Solid State Chem. 36: 372-380.